Chapter 4

Dynamics of martian meteoroids

In order to calculate the expected flux of martian meteorites, either in a relative or absolute sense, we must first calculate the delivery efficiency for martian material (the fraction of escaping material that arrives at the Earth).

4.1 Introduction

Martian meteorites have taken much longer to reach the Earth than the lunar ones (Table 2.1, page 16), simply because the orbits of most ejected martian meteoroids do not initially cross that of the Earth. However, because of the eccentric orbit of Mars, the v_∞ of escaping particles need only be about 2.3 km/s (corresponding to ejection speeds of 5.5 km/s, merely 10% greater than the 5 km/s escape speed) in order for some ejecta to be on orbits that immediately cross Earth's. Thus, fast transfers are occasionally possible and the short 0.6 Myr 4π CRE age of EET79001 is not especially surprising. In fact, transfers as rapid as 16,000 yr were observed in the simulations.

The ground-breaking work of Wetherill (1984), who a decade ago addressed the delivery efficiency of martian meteorites using Monte Carlo simulations, presents, in hindsight, a puzzle given what we now know of the 4π CRE ages of these meteorites. Even though collisional destruction was included in those simulations, the majority of martian objects arrived at the Earth having taken longer in their journeys than the recovered meteorite with the greatest CRE age ($\approx$15 Myr), unless the mean ejection velocities are very large indeed ($>$ 6.4 km/s). Since the lunar results seem to indicate that proportionally little material is launched at speeds greater than 125% of the escape speed, one might expect that most martian meteoroids should be launched at $<$ 6 km/s. Of course, it may

* This chapter is a considerably expanded version of discussion given in the paper: Gladman, B., J.A. Burns, M. Duncan, P. Lee, and H. Levison (1996), The Exchange of Impact Ejecta Between Terrestrial Planets, *Science* **271**, 1387–92 [copyright 1996 by the American Association for the Advancement of Science].

be that the regolithic structure of the lunar surface is responsible for the sharp drop-off with velocity, and that this result does not apply to Mars. However, Vickery (1987) studied secondary crater fields around martian, lunar, and mercurian impact craters and found power-law decreases in the fragment size with increasing ejection speed that had little variation between the planetary bodies.

4.2 Simulations

I have simulated the gravitational evolution of 2100 particles escaping from Mars at various speeds, for up to 100 Myr. The planets from Venus to Neptune were included in the simulations. The initial conditions for the test particles consist of placing the test particles uniformly on the surface of a sphere 100 martian radii away from the planet, moving radially outward at a chosen velocity v_∞ (this corresponds to uniform cratering of the planet). Previous work (Wetherill 1984) has shown that the delivery efficiency is relatively insensitive to the orbital phase and current orbital elements of Mars. Ejection from the planet results in the escaping particles being in heliocentric orbit immediately; no intermediate phase of orbit around the planet need be considered. Particles were removed for the same reasons as in the lunar case: planetary collision, $Q > 6$ AU, or Sun-grazing. The Sun-grazing criterion was changed to the actual solar radius (*i.e.*, $q = 0.005$ AU); the frequency of Sun-grazing was found to be insensitive to whether one or two solar radii were used as the termination distance.

The depletion rate of the ejected particles (Fig. 4.1) is clearly different from the other cases (launch from Mercury and Venus is discussed in Chpt. 5) because, even at this low ejection speed, re-collision with Mars is not a significant removal mechanism. Of the few Mars re-impacts that do occur, more than 90% take place in the first few Myr; once the relative velocities increase above the escape velocity, collisions with Mars remove an insignificant fraction. For higher ejection speeds, typically less than 2% of the particles re-collide.

The delivery efficiency of martian meteoroids to the Earth for $v_\infty = 1$ km/s is $\simeq 7.5\%$, with about one-third of these occurring in the first 10 Myr (Table 4.1). Interestingly, Mars, Venus, and Earth all receive comparable fractions of the material ejected from Mars. Raising the ejection velocity causes a small increase in the delivery efficiency to Earth (Table 4.2). The yields shown here are about an order of magnitude larger than those seen in Monte Carlo simulations (Wetherill 1984), although I have not yet included the possibly important effects of collisional destruction. These collisional effects lower the transfer efficiency by a factor of 2 at most, but this still results in a significant difference with the Monte Carlo results. The discrepancy can be understood by examining Fig. 4.2, which shows how the orbits of the escaped ejecta evolve after launch. It can be seen that the particles remain in the vicinity of Mars ($a = 1.52$ AU) only for the first 100,000 years. By 1 Myr several interesting phenomena have occurred: a few particles

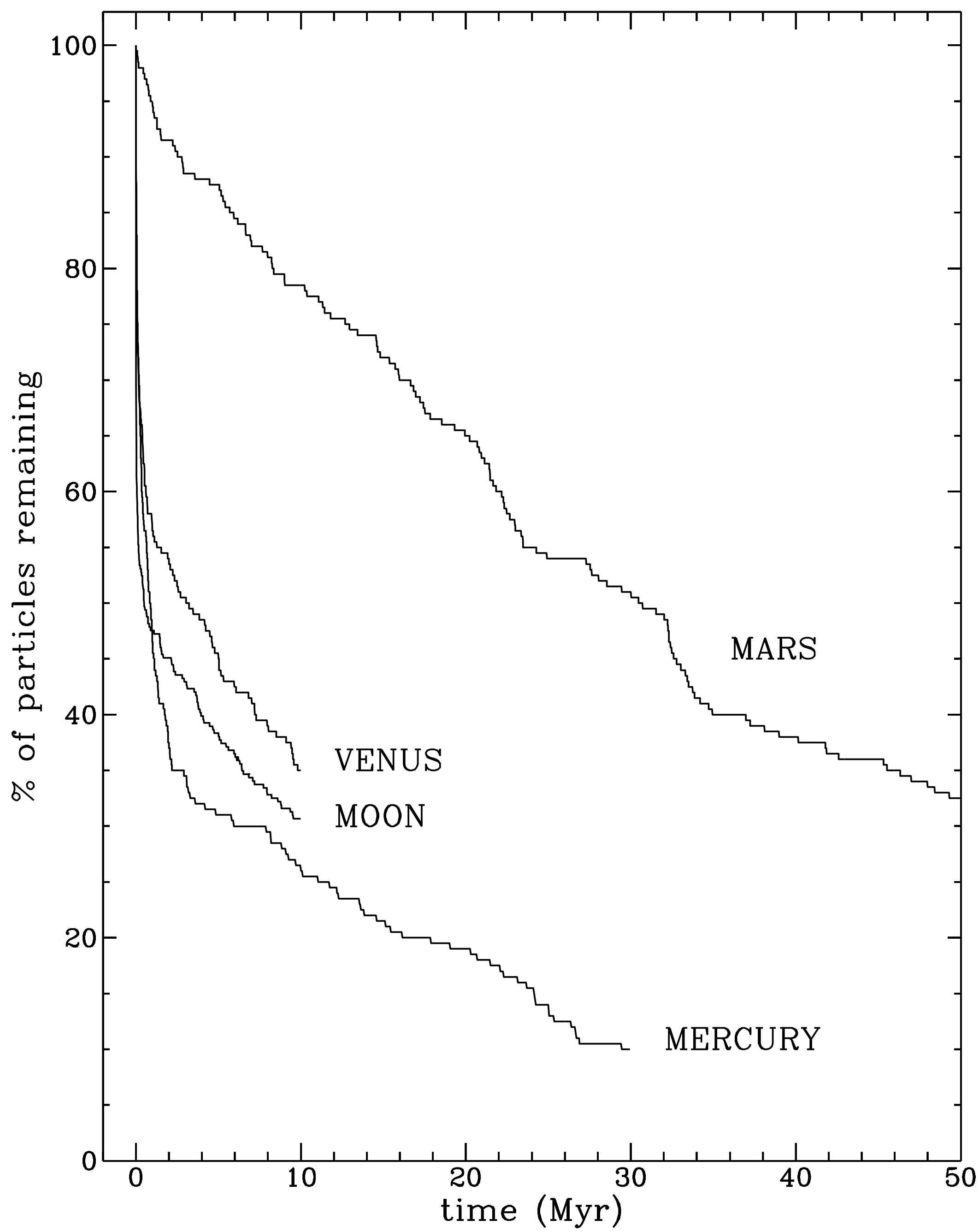

Figure 4.1 The fraction of escaping particles remaining in the simulations as a function of time. The simulations for Mercury, Venus, and Mars are the $v_\infty = 1$ km/s cases, while the lunar simulation shown is for an ejection speed v_l off the lunar surface of 2.4 km/s.

Table 4.1 Fates of the particles from a compilation of five v_∞=1 km/s martian ejecta simulations containing a total of 900 particles and lasting up to 100 Myr. No collisional effects are included in these simulations.

Meteoroid fate	Fraction
Impact Venus	7.5%
Impact Earth	7.5%
Impact Mars	9.0%
Sun-grazing	38%
Reach Jupiter	15%
Survivors	23%

Table 4.2 Transfer efficiencies for Mars ejecta in the first 15 Myr after launch, as a function of the ejection speed, with no correction for collisional destruction. All simulations used 300 particles. (*) Note that Sun-grazing and Jupiter-crossing only begin to operate efficiently after 10 Myr, and thus are under-represented here (compare with Table 4.1).

Ejection speed (km/sec)		Efficiency, in 15 Myr (%)				
v_∞	Surface	Earth	Venus	Mars	Sun*	Jupiter*
1.0	5.13	3.1	1.5	9.5	9.0	3.0
1.8	5.34	4.0	2.7	2.7	8.0	6.0
2.3	5.53	7.7	4.7	0.7	9.0	5.0
2.7	5.71	5.3	4.0	1.7	9.3	5.0
3.3	6.02	6.3	3.7	2.0	13.3	6.7

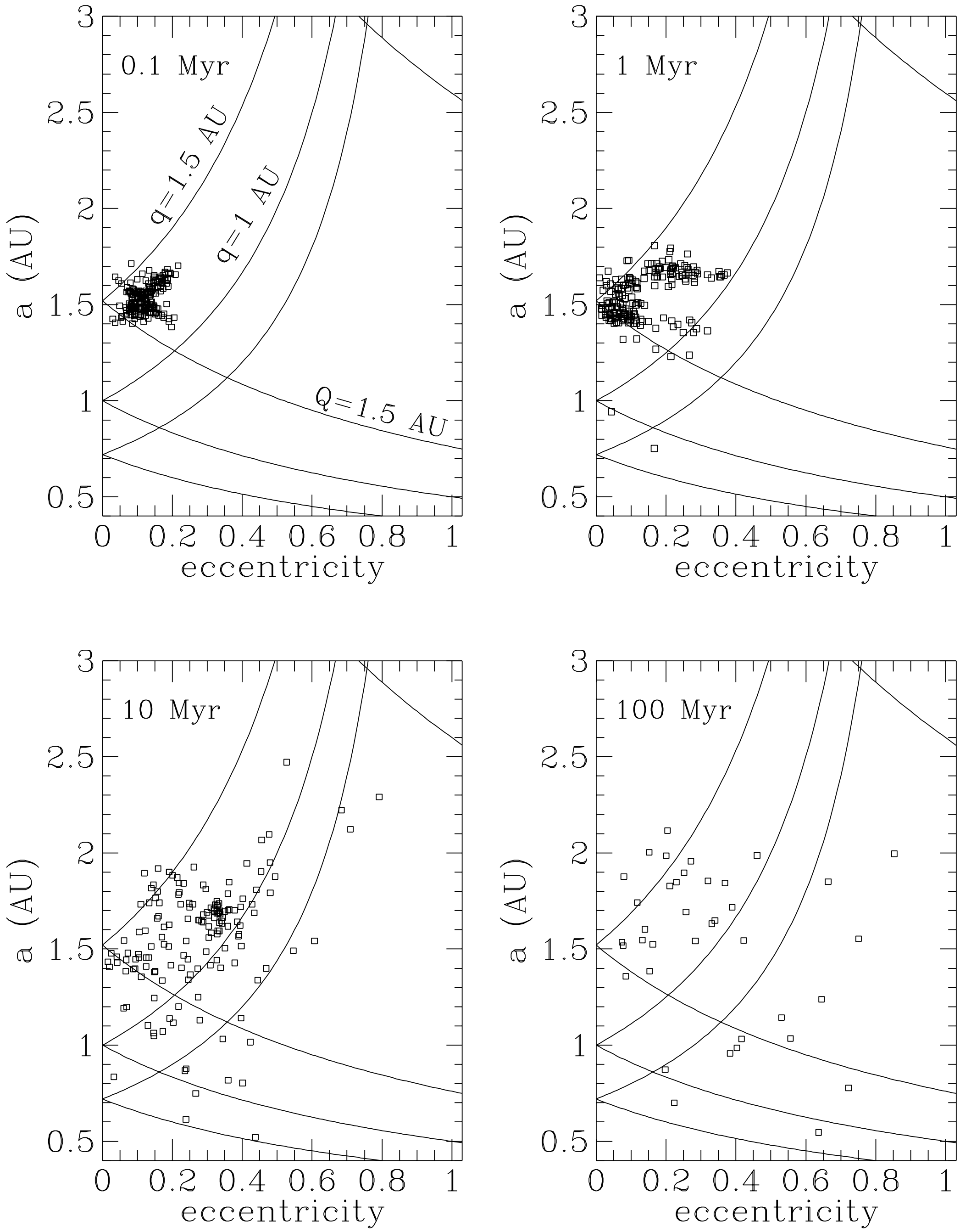

Figure 4.2 Orbital evolution of 200 particles launched from Mars with v_∞=1 km/s. The web of lines shows the locations where the perihelion or aphelion of a particle would lie at a planet's semimajor axis (the curve in the upper right corresponding to Jupiter).

have diffused down the $Q = 1.5$ AU line due to multiple close encounters (in a manner similar to that observed in the lunar simulations), and some of these particles have had their orbits drastically modified by the Earth (having crossed the $q = 1$ AU line). The obvious feature at $a \simeq 1.65$ AU is caused by secular resonances discussed in the next section. By 10 Myr most of the particles have been removed from Mars-like orbits, and by 100 Myr it is apparent that the population has been heavily depleted.

4.2.1 Secular resonances near Mars

Unlike the lunar simulation, diffusion up the $q = 1.5$ AU line is halted by the presence of two nonlinear, second-order secular resonances, which are thought to be located near $a \simeq 1.6 - 1.7$ AU using a perturbation theory calculation (Froeschlé and Morbidelli 1994). The resonances are $2g = g_5 + g_6$ and $g - s = g_5 - s_6$, with the former the more dynamically effective of the two. The libration of the two resonant arguments is shown for one of the test particles in Fig. 4.3. Note that in these figures the plotted resonant angle is indicated by the resonant frequency (*e.g.,* the angle $2\tilde{\omega} - \tilde{\omega}_5 - \tilde{\omega}_6$ is plotted in the $2g = g_5 + g_6$ panels. Here g and s denote the precession rates of the perihelion and ascending node of the particle, and g_i and s_i are the i^{th} fundamental secular eigenfrequencies of the solar system (Brouwer and Clemence 1961). First-order secular resonances occur when a single secular frequency is matched; for example, if $g = g_5$ then the particle's pericenter precesses at the same rate that Jupiter's does and the particle would be in the classical ν_5 resonance (the two notations are equivalent). In the current case the resonances are non-linear because they involve more than one fundamental frequency, and second-order because they do not appear in the expansion of the secular disturbing function until quadratic terms in the planetary masses are considered.

These resonances cause oscillations, with periods of $\sim 10^5$ yr, in the eccentricities of particles in this region up to Earth-crossing values ($e \simeq 0.4$) thereby raising the efficiency of delivery for martian meteoroids (Fig. 4.4). Since these resonances were not incorporated into earlier Monte Carlo simulations and appear to have such dramatic effects, it is not surprising that the results differ. These two secular resonances appear to be present in much of the phase space near the martian region; a large fraction of the particles (at many different values of a, e, and i) have precession rates (presumably induced by Mars) matching one of these secular frequencies, even though they may not be at the locations determined by Froechlé and Morbidelli (1994). Fig. 4.4 illustrates that particles can be at a variety of semimajor axes and eccentricities and still be locked in these resonances.

Besides the potential for Earth impact, another consequence of the delivery of particles to the $q = 1$ AU curve is that their semimajor axes can be raised by

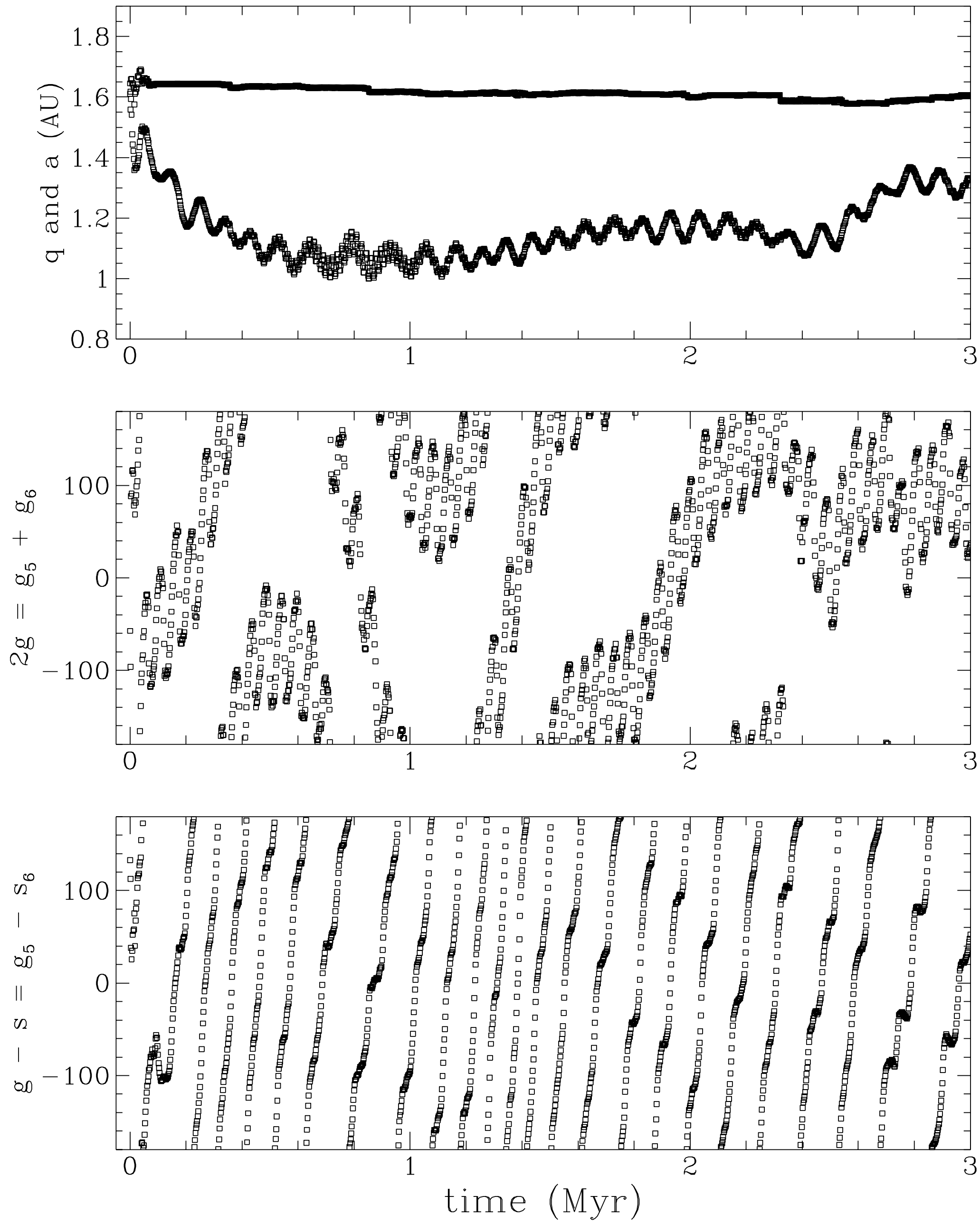

Figure 4.3 An orbital history of a martian meteoroid. The semimajor axis and perihelion distance are shown. This particle spends the duration of this simulation with an inclination $i < 20°$, and with ω and Ω circulating. The resonant angles indicate that the particle is near, but not exactly at the two second-order secular resonances, which nevertheless quickly increase its eccentricity to 0.3, and the particle becomes mildly Earth-crossing. The perihelion then decouples from the Earth, although the particle then firmly locks in the $2g = g_5 + g_6$ resonance.

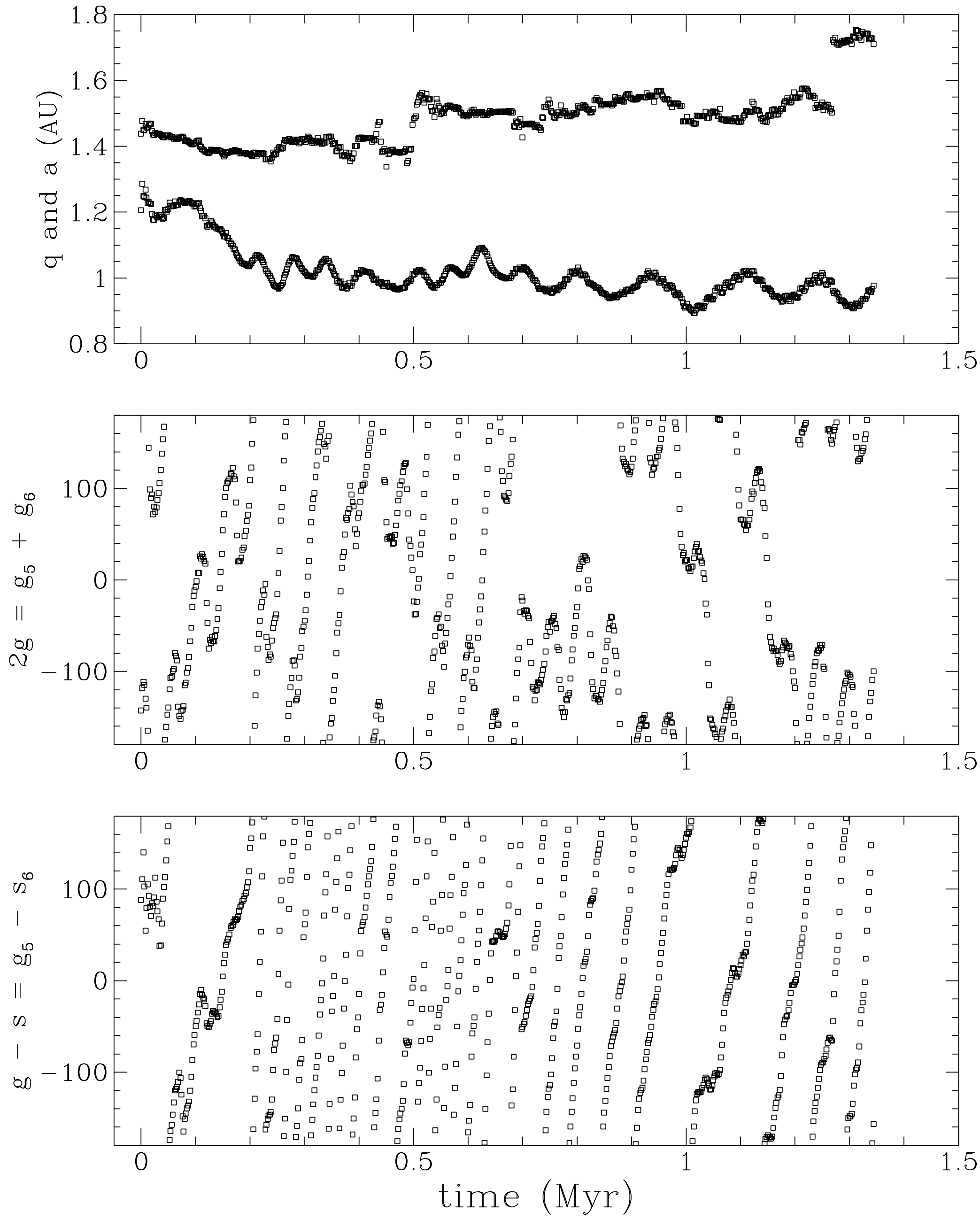

Figure 4.4 Libration of the two second-order secular arguments for a martian meteoroid that impacts the Earth. This particle appears to begin the simulation in the resonances (as indicated by the libration of the resonant angles), and they cause the eccentricity e to rise and thus perihelion q to be lowered to Earth-crossing values (the top panel also shows the semimajor axis a). The particle spends most of its lifetime locked in the $2g = g_5 + g_6$ resonance. Even the close encounter at $t \simeq 1.27$ Myr does not disrupt the resonant behavior. At $t = 1.38$ Myr the particle collides with the Earth.

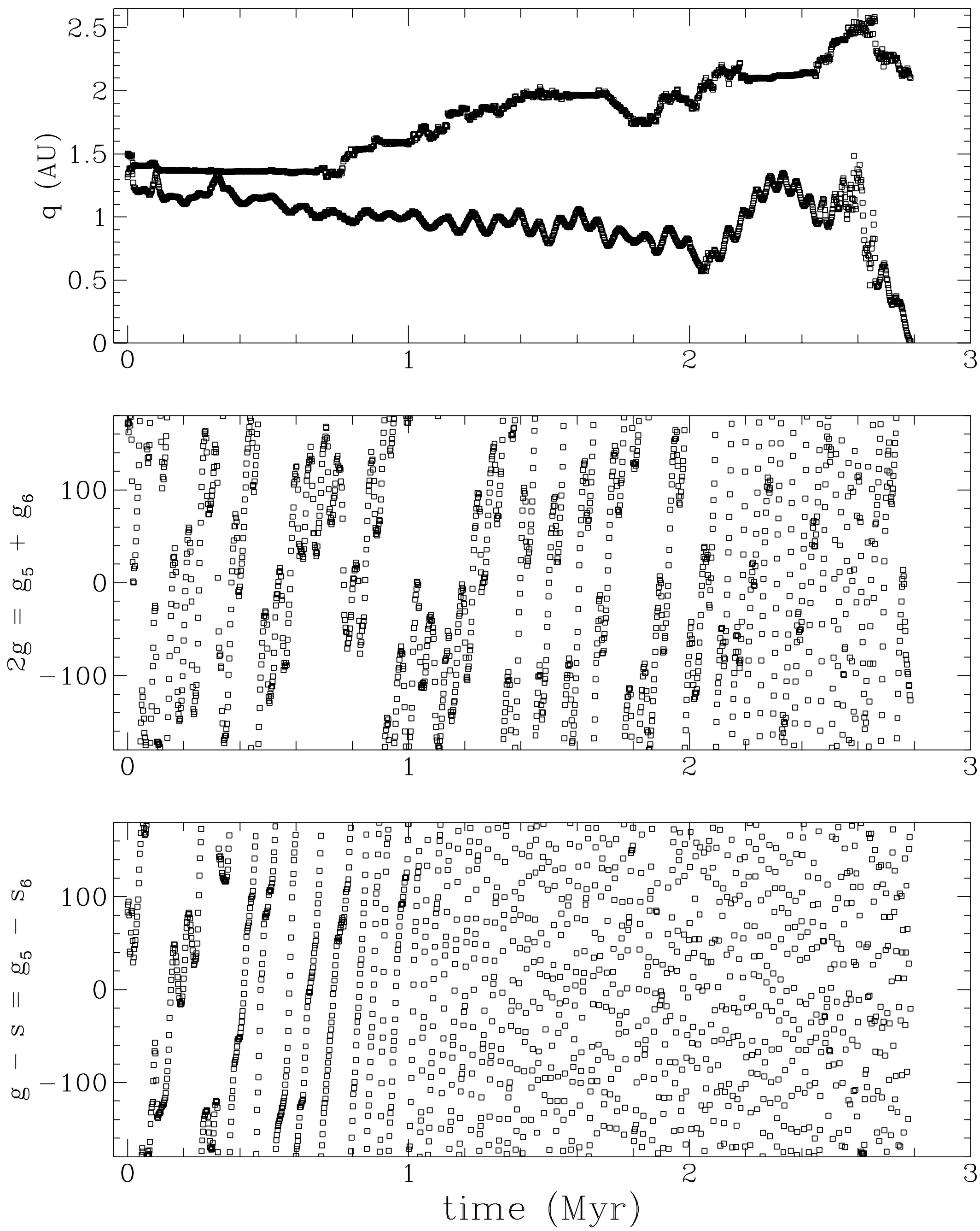

Figure 4.5 Libration of the two second-order secular arguments for a martian meteoroid that becomes a Sun-grazer. Starting at $t = 2.6$ Myr the eccentricity is driven to unity and the particle impacts the Sun. The other orbital elements and resonant arguments are shown in Fig. 4.6; note especially the resonant angle for the ν_6 resonance.

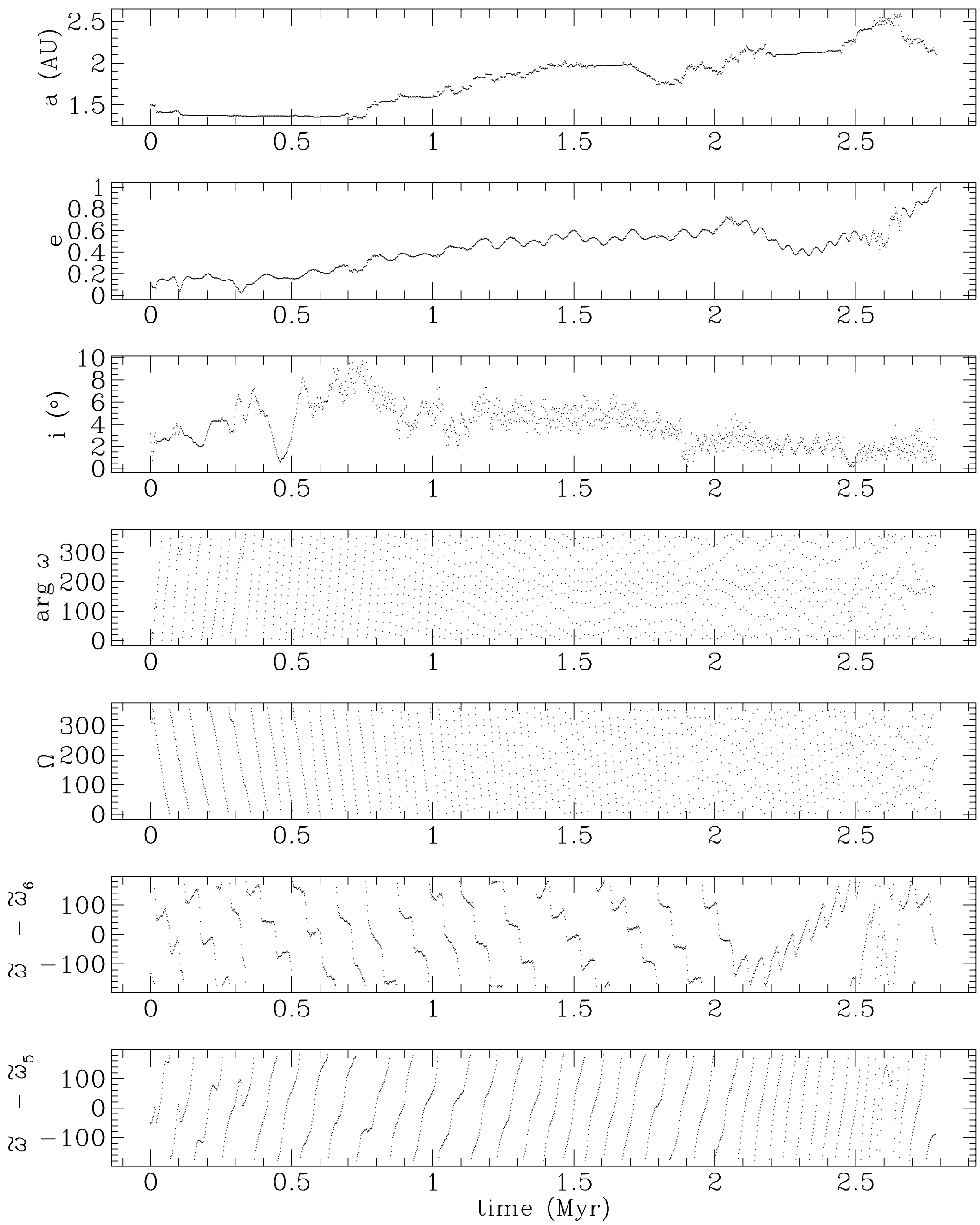

Figure 4.6 The other orbital elements for a martian meteoroid that becomes a Sun-grazer. This is the same particle as in Fig. 4.5. Note that ν_5 and ν_6 resonances are important near the end of the evolution; the eccentricity rises rapidly when the semimajor axis reaches $a > 2$ AU and both ν_5 and ν_6 are important. Note also that the particle seems to leave $2g = g_5 + g_6$ at 2.1 Myr when it becomes locked in ν_6.

close encounters (with the Earth and Venus) to the inner edge of the asteroid belt ($a \simeq 2.1$ AU), where the powerful secular resonances ν_6, ν_5, and ν_{16} operate; these resonances are capable of driving the eccentricities of test particles to unity at which point the particles strike the Sun, as discussed previously. Sun-grazing is discussed for near-Earth asteroids by Farinella *et al.* (1994), for the short-period comets by Bailey *et al.* (1992), and for the Jupiter family comets by Levison and Duncan (1994).

Sun-grazing (illustrated in Figs. 4.5 and 4.6) is in fact by far the dominant loss mechanism after 10 Myr. By 100 Myr almost 40% of the particles have been driven into the Sun, more than twice the number removed from the system by crossing Jupiter's orbit. These two effects ultimately deplete the swarm and yield an almost linear decline in the number of surviving meteoroids (Fig. 4.1); this partly explains why no martian meteorites have 4π ages older than ~ 15 Myr; collisional effects, which also contribute, will be discussed in the next section.

To conclude our discussion of the simulations, Fig. 4.7 presents cumulative spectra (over 15 Myr of evolution only) for the simulations presented in Table 4.2. In contrast to the lunar case, the delivery rate of martian meteorites to the Earth appears to be almost constant (note the linear time axis, as opposed to the logarithmic one for the lunar case of Fig. 3.13). Given the relatively small number statistics of the simulations there is little difference between the launch velocities. The only slight difference is that the $v_\infty = 2.3$ km/s case has an increase in early deliveries due to the fact that at this value of v_∞ a fair number of particles have $q \simeq 1$ AU at the very beginning of the heliocentric simulation, allowing almost immediate deliveries.

4.3 Comparison with meteorite data

Fig. 4.8 shows, in a cumulative plot, the expected CRE age spectrum for the purely gravitational N-body simulation with $v_\infty = 1$ km/s, which was run for 100 Myr of simulated time in order to extend well past the 4π age of the oldest martian meteorite. The agreement with the martian meteorite data does not appear to be as good as in the lunar case; only a little more than half of the meteorites delivered in the simulation arrive within the 15-Myr upper bound of the recovered meteorites (a problem mentioned in Sec. 1.5). However, this disagreement is not surprising at this stage. The delivery time scale is many millions of years (as opposed to tens to hundreds of thousands of years for the lunar meteorites). Many of the martian meteoroid orbits reach out to the asteroid belt ($Q > 2.1$ AU) for at least some of the time during their journey to the Earth and thus the meteoroids will be prone to collisional disruption, with a half-life of $\sim$ 1–10 Myr (Bottke *et al.* 1994). This is in rough agreement with the observed CRE ages of the ordinary chondrites (Wasson 1985). Wetherill (1988) postulates

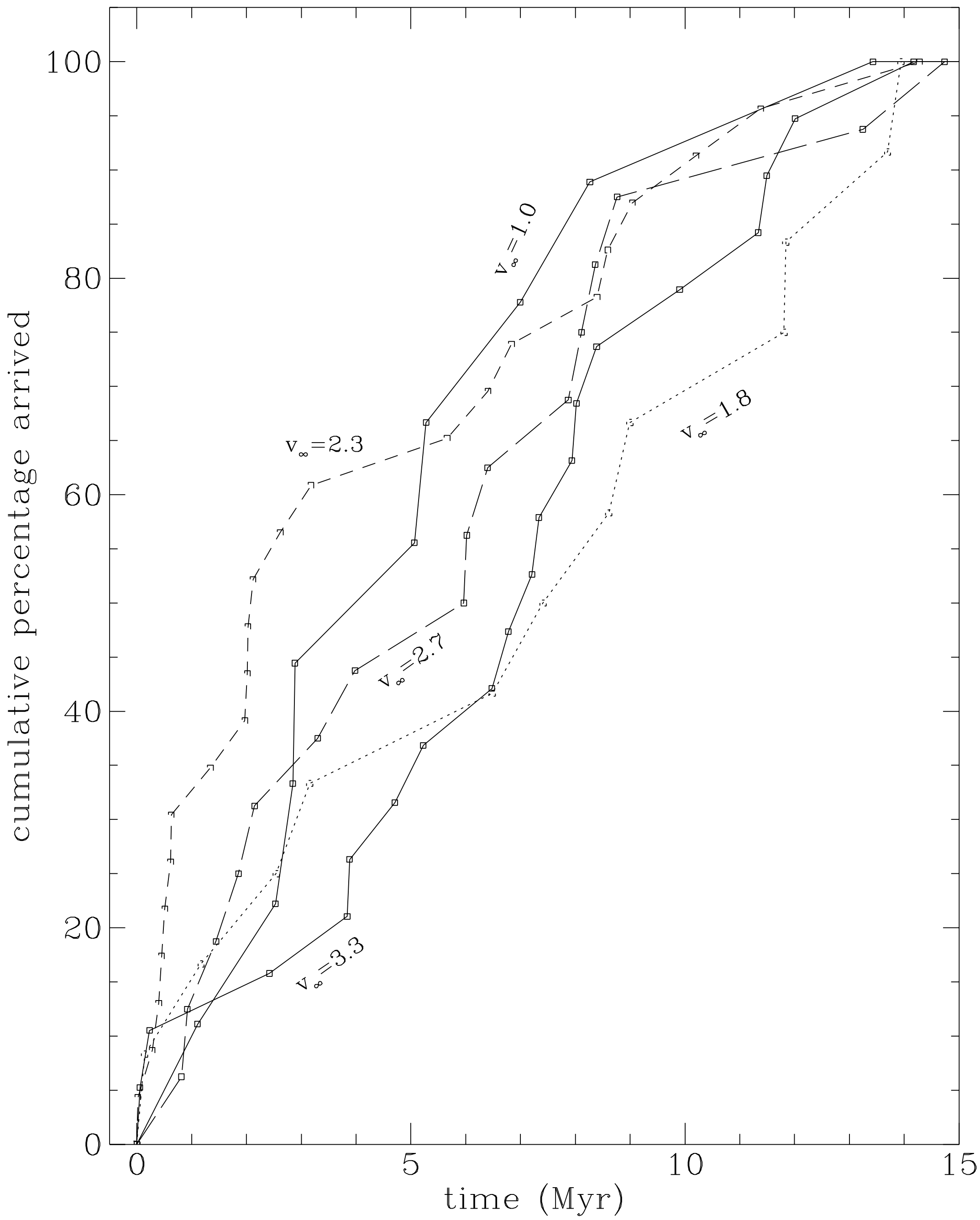

Figure 4.7 Cumulative delivery spectra for all 15 Myr martian simulations. The vertical axis is the cumulative fraction of objects that have struck the Earth, *of all those that will within 15 Myr*. The points shown represent each individual impact seen in the simulation (of 300 particles). Given the relatively small number of deliveries, these spectra are all well represented by a constant delivery rate, although note that the total efficiency varies by a factor of about 2 (Table 4.2).

a collisional half-life for a meteoroid of radius r (in cm) of

$$\tau_{\rm coll} = 1.2 \times 10^6 \; r^{1/2} \;\; {\rm yr}, \tag{4.1}$$

when $Q > 2.1$ AU. Thus a $r \simeq 3$ cm meteoroid (pre-atmospheric mass ~ 300 g) with aphelion in the main belt would have a collisional lifetime of only 2 Myr. Since the half-life scales only as $\sqrt{r}$, the range of a factor of 10^3 in martian meteorite masses corresponds to a variation of only a factor of 3 in $\tau_{\rm coll}$. Even the 40-kg Nakhla meteoroid would have had a collisional half-life of no more than ~ 5 Myr if it entered the main belt. Thus I have used the value of 2 Myr (roughly the lifetime for the median martian meteorite mass) for all meteoroids; further refinements are unwarrented in any case given the small numbers of meteorites.

The time spent in the main asteroid belt as a function of transit time to the Earth was tabulated from the simulations (Fig. 4.9). It is apparent that most meteoroids that arrive at the Earth in less than 10 Myr spend little, if any, time transiting through the main belt. On the other hand, most objects taking more than 10 Myr to arrive at the Earth spend many millions of years in the main belt, and are unlikely to survive this given their small sizes. (Chondrites with CRE ages of tens of Myr are known, but this cosmic ray exposure was almost certainly acquired while the material was in roughly meter-sized bodies, in concordance with Eq. 4.1).

I am assuming a model in which hypervelocity collisions into martian meteoroids smaller than several tens of kilograms are so catastrophic that no collisional products are capable of surviving until Earth delivery (if this were not true, then we should presumably have martian meteorites with transit ages as old as the oldest chondrites). The mean residence time in the belt was calculated from Fig. 4.9 as a function of transit time (using 3-Myr bins) and convolved into the delivery spectrum (Fig. 4.8). With such a collisional model, the N-body simulation matches the CRE data reasonably well; however, the collisions lower the delivery efficiency for the $v_\infty = 1$ km/s case from 7.5% to $\simeq 3\%$.

4.4 Implications for the launch process

The age distribution of the martian meteorites is consistent with a model in which all fragments are launched, at speeds modestly above the escape velocity, as small bodies and delivered independently to Earth. The orbital elements just before impact of the particles in one of the v_∞=1 km/s simulations are shown in Fig. 4.10. The simulated meteorites delivered in the first 15 Myr almost all have entry velocities into Earth's atmosphere in the range 11–17 km/s (Fig. 4.11), in agreement with the ablation data for the SNCs (Bhandari *et al.* 1988). In fact, there is some cosmogenic nuclide evidence that the quickly arriving shergottites have systematically lower ablation than the other martian meteorites (Garrison

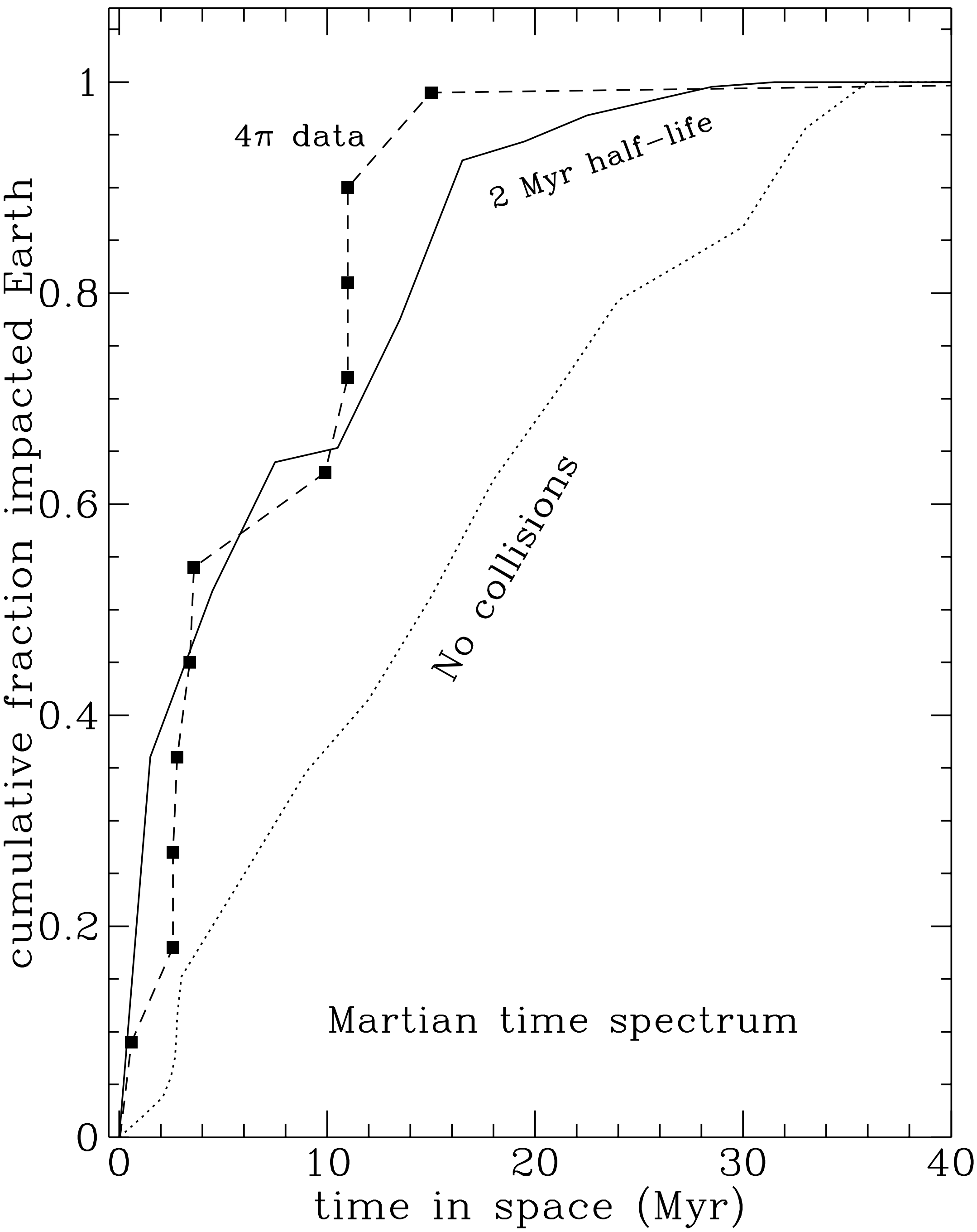

Figure 4.8 Cumulative plot of the expected CRE age spectrum of the martian meteorites. The curves show (as a function of time) the cumulative number of meteorites that have struck the Earth (as a fraction of those that do within 40 Myr. The solid and dotted curves show predicted spectra, one incorporating catastrophic collisions (solid) and the other without (dotted). The dashed line connects the data points for the martian meteorites.

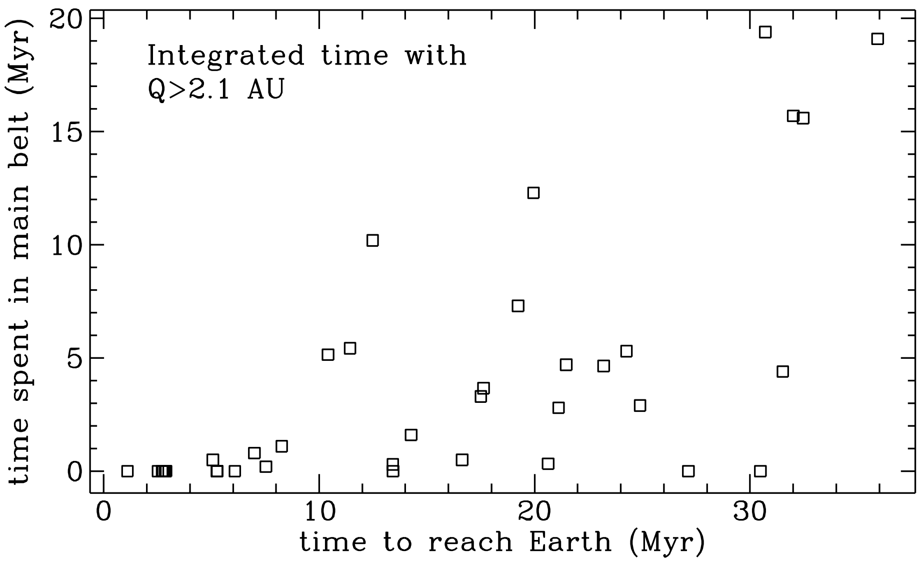

Figure 4.9 For the particles that struck the Earth in the first 40 Myr of the 100-Myr, v_∞=1 km/s simulation, the integrated amount of time spent in the main asteroid belt is plotted as a function of the time it took for the meteoroid to reach the Earth. (Only 1 particle struck the Earth after this, at $t = 73$ Myr).

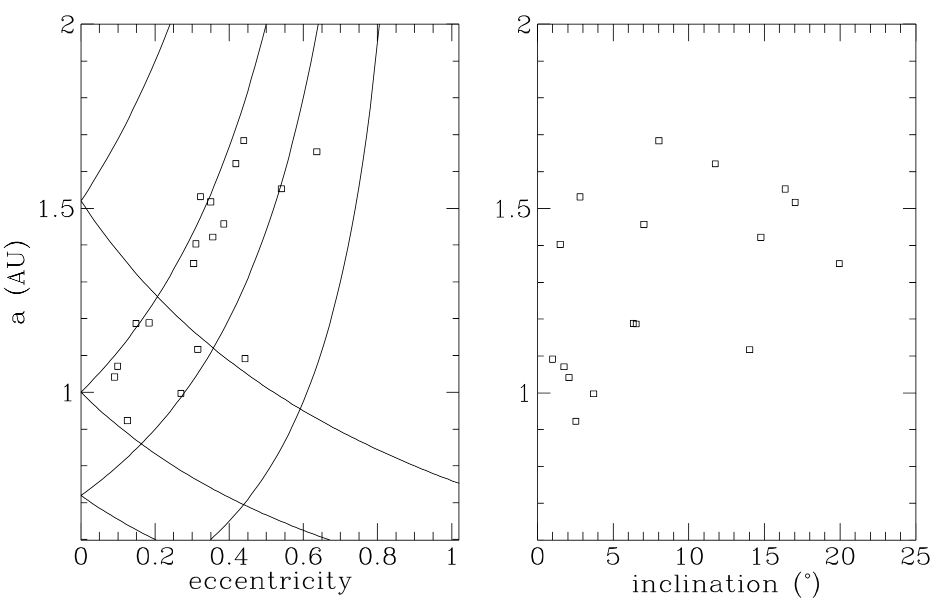

Figure 4.10 The orbital elements just before impact of the simulated meteorites from one of the 100-Myr simulations.

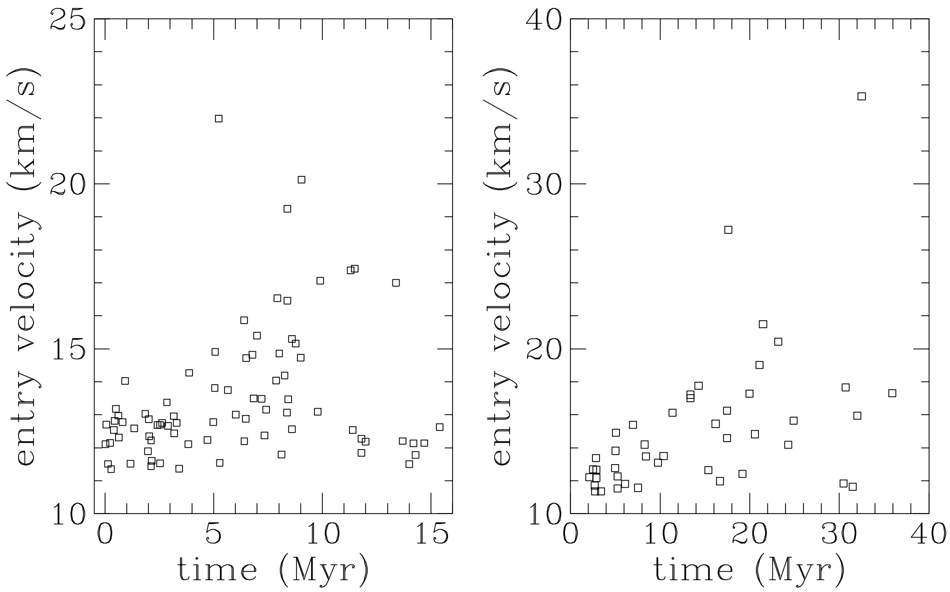

Figure 4.11 The entry velocities for the simulated martian meteorites that reach the Earth. Left panel: All particles from the 15-Myr simulations. Right panel: particles from the 100-Myr simulation. Note the differing axes.

et al. 1995, Swindle *et al.* 1996). This tendency is definitely supported by the simulations; Fig.4.11 shows atmospheric entry velocities at the Earth for the meteorites from all of the 15-Myr simulations as well as the 100-Myr simulation. Meteorites arriving as rapidly as the shergottites (<4 Myr) seldom seem to have atmospheric entry velocities greater than the relatively low value of 13 km/s, which would result in ablative mass losses of 40–60% (ReVelle 1979), corresponding to about 20% of the meteoroids radius. This could explain the systematically lower ablation seen in the shergottites (Garrison *et al.* 1995).

However, the simulations do not explain the apparent clustering of the 4π CREs into at least 3 groups: 0.6 Myr (1 object), 3 ± 1 Myr (5 objects), and 13 ± 3 Myr (5 objects). Are these groups due to source-crater pairing (p. 2) or, alternatively, to separate collisional fragmentations of large meteoroids in space (Bogard 1995)? Note that the cumulative spectrum (Fig. 4.8) would be unchanged by source-crater pairings. Tremain and co-workers (Tremain *et al.* 1994, Tremain 1995a) argue for one-stage exposures as small bodies, but allow for source-crater pairing of the shergottites or nakhlites/Chassigny. The martian meteorites share much closer petrologic affinities than the lunar meteorites (McSween 1995): the 3-Myr group contains only shergottites, and 3 of the 13-Myr group are the nakhlites. Recently, Eugster (1996) claims the following source-crater pairings on the basis of CRE evidence: three of the basaltic shergottites (Shergotty, Zagami, and QUE94201) at $\simeq 2.7$ Myr ago, the two lherzolitic shergottites at $\simeq 3.5$ Myr ago, and all three nakhlites at $\simeq 10.5$ Myr ago (*cf.* Tables 1.2 and 2.1). I agree that these age clusters likely represent individual impact events into distinct source terrains (see Chpt. 6).

A previously considered hypothesis (Vickery and Melosh 1987) – that all the martian meteorites are derived from recent catastrophic fragmentations of large bodies that were launched 200 Myr ago and then stored in space – is rendered very unlikely since the simulations demonstrate that few parent bodies can dynamically survive for this time owing to the efficiency of meteoroid destruction, especially by Sun-grazing. This model would also have to explain why (i) there are no meteorites from the upper few meters of the parent meteoroids (half of even a 10-m meteoroid is within 2 m of its surface and thus exposed to cosmic rays!), (ii) no impacts more recent than 200 Myr have been sampled, and (iii) only shergottite parent meteoroids have been disrupted in the last 3 Myr, and none before. The results presented here show that the simpler model, which produces exclusively small meteoroids, explains all the CRE evidence, although source-crater pairings and relative surface properties of the Moon compared to Mars may be important. The issues of why such groupings occur for Mars but not for the Moon and why there are equal numbers of lunar and martian meteorites (Wetherill 1984) remain, and will be considered in Chap. 6.